International Journal of Digital Earth

ISSN: 1753-8947 (Print) 1753-8955 (Online) Journal homepage: www.tandfonline.com/journals/tjde20

A combined image matching method for Chinese optical satellite imagery

Yansong Duan, Xu Huang, Jinxing Xiong, Yongjun Zhang & Bo Wang

To cite this article: Yansong Duan, Xu Huang, Jinxing Xiong, Yongjun Zhang & Bo Wang (2016) A combined image matching method for Chinese optical satellite imagery, International Journal of Digital Earth, 9:9, 851-872, DOI: 10.1080/17538947.2016.1151955

To link to this article: https://doi.org/10.1080/17538947.2016.1151955

INTERNATIONAL JOURNAL OF DIGITAL EARTH, 2016
VOL. 9, NO. 9, 851–872
http://dx.doi.org/10.1080/17538947.2016.1151955

Taylor & Francis
Taylor & Francis Group

A combined image matching method for Chinese optical satellite imagery

Yansong Duan[a], Xu Huang[a], Jinxing Xiong[b], Yongjun Zhang[a] and Bo Wang[c]

[a]School of Remote Sensing and Information Engineering, Wuhan University, Wuhan, Hubei, China; [b]2012 Laboratory of HUAWEI Technology Co., Ltd., Shenzhen, China; [c]College of Astronautics, Nanjing University of Aeronautics and Astronautics, Nanjing, Jiangsu, China

ABSTRACT

Image matching is one of the key technologies for digital Earth. This paper presents a combined image matching method for Chinese satellite images. This method includes the following four steps: (1) a modified Wallis-type filter is proposed to determine parameters adaptively while avoiding over-enhancement; (2) a mismatch detection procedure based on a global-local strategy is introduced to remove outliers generated by the Scale-invariant feature transform algorithm, and geometric orientation with bundle block adjustment is employed to compensate for the systematic errors of the position and attitude observations; (3) we design a novel similarity measure (distance, angle and the Normalized Cross-Correlation similarities, DANCC) which considers geometric similarity and textural similarity; and (4) we introduce a hierarchical matching strategy to refine the matching result level by level. Four typical image pairs acquired from Mapping Satellite-1, ZY-1 02C, ZY-3 and GeoEye-1, respectively, are used for experimental analysis. A comparison with the two current main matching algorithms for satellite imagery confirms that the proposed method is capable of producing reliable and accurate matching results on different terrains from not only Chinese satellite images, but also foreign satellite images.

ARTICLE HISTORY
Received 10 July 2015
Accepted 3 February 2016

KEYWORDS
Image matching; Chinese satellite imagery; mismatch detection; integrated similarity measure; improved Wallis filter

1. Introduction

Digital Earth is a multi-resolution, multi-dimensional representation of the virtual planet with vast quantities of geo-referenced information, which was proposed in Gore's 1998 speech. In recent years, digital Earth has attracted a lot of attention with the technical feasibility, including digital elevation model or digital surface model (DSM) generation, 3D GIS analysis and the representation of digital Earth (Goodchild 2008). The generation of digital Earth model is a necessary technology because both the 3D GIS analysis and the representation cannot be carried out without the help of the virtual planet model. Image matching is one of the effective ways to acquire the model of digital earth, which recovers three-dimensional coordinates of ground surface from images. Images can come from different sensors and platforms including satellites, airplanes, unmanned aerial vehicles and motor vehicles, among which satellite images are widely used in digital earth for their wide coverage area, short revisit cycle, and high spectral resolution. Foreign satellites such as QuickBird, IKONOS and GeoEye have provided vast amounts of images for various digital Earth applications.

With the rapid development of space technology and the important breakthrough of satellite positioning techniques, the number of satellites in orbit has risen markedly in China (Cheng,

CONTACT Yongjun Zhang zhangyj@whu.edu.cn School of Remote Sensing and Information Engineering, Wuhan University, No. 129 Luoyu Road, Wuhan 430079, Hubei, China

Deng, and Li 2010; Guo 2012). More and more satellite data can now be applied in photogrammetry and remote sensing, such as the images from Mapping Satellite-1, the ZY-1 02C and ZY-3 satellites. Although it can be seen that the performance of Chinese satellites has improved substantially, some gaps still exist when they are compared to foreign satellites. The camera errors caused by lens distortion, CCD (Charge Coupled Device) bending and misalignment of sub-CCD arrays are not insignificant (Zhang et al. 2014; Zheng et al. 2015). Moreover, the direct georeferencing accuracy using the original position and attitude data is low (Xie 2009). According to the test results produced from the ZY-3 satellite data, the absolute accuracy of direct georeferencing before orientation was about 1300 meters in plane and 300 meters in height, and the internal accuracy was about 200 pixels (Zhang et al. 2014).

With the development of Chinese industry, air pollution in China is becoming more and more serious. In recent years, atmospheric particles, e.g. PM 2.5, have become the culprit of the air pollution in Chinese urban areas. The atmospheric particles can decrease the quality of satellite imagery (Srinivasa and Shree 2002). Due to the limitation of Chinese sensor hardware and the air pollution, the image quality of Chinese optical satellites in urban area in China is not satisfactory, which will bring challenges for image matching.

Due to the differences between Chinese satellite data and foreign satellite data, the existing matching methods which have been used in foreign satellite data successfully need more experiments to test if they can be applied to Chinese satellite data. Image matching, a key technology in photogrammetry, is used in aerial triangulation, DSM generation, etc. In the past 20 years, many empirical matching algorithms for satellite imagery have been proposed, but their performance remains unsatisfactory, and, in some cases, it is far from acceptable (Gruen 2012). The following current problems need to be solved:

(1) Since the exterior orientation parameters (EOPs) of satellite images are known in advance, epipolar lines are employed as a spatial constraint (Zhang and Gruen 2006) by many matching algorithms. However, the errors in the real-time EOPs for Chinese satellite images are large, which causes the low prediction accuracy of epipolar lines. When there is a large disparity between the correspondences and their corresponding epipolar lines, the mismatches increase substantially.
(2) There are large local geometric distortions between satellite images acquired from different platforms and perspectives. These distortions may decrease the correlations between correspondences and may make matching algorithms invalid as well.
(3) For difficult matching situations such as residential areas, mountainous, poor textural areas and woodland areas, it is difficult to find reliable correspondences, and some algorithms may not even work (Wu, Zhang, and Zhu 2012).

According to the problems above, we propose a combined image matching method for Chinese satellite imagery. The large errors in the real-time EOPs for Chinese satellite images can be reduced by initial geometric orientation described in Section 3.2. In Section 3.3.2, we introduce a method to rectify the problem of large local geometric distortion. In Section 3.3.3, a new similarity measure is proposed to solve the problem of difficult matching situations.

The rest of the paper is arranged as follows: a literature review on algorithms for matching satellite images is first presented in the following sections, followed by an illustration of the algorithmic outline; after the details of the proposed method are described, the experimental results are analyzed; finally, concluding remarks and future research are discussed.

2. Related work

Image matching is used to looking for conjugate points of overlapping pictures (Joz et al. 2012). The results of matching will influence the performance of bundle adjustment for Chinese satellite directly

(Zhang et al. 2015). For the past 30 years, it has been one of the most challenging tasks in photogrammetry (Heipke 1996; Mustaffar and Mitchell 2001). However, there have been some impressive algorithms on matching with satellite imagery. Gruen and Baltsavias (1988) developed the 2-view matching algorithm to multi-views and proposed the Multi-Photo Geometrically Constrained matching algorithm, which was an extension of the Least Square Matching (LSM) algorithm (Ackermann 1984). This algorithm compensates for the distortions caused by imaging geometry and terrain relief. The strict geometric and radiometric assumptions for the NCC method (Helava 1978; Lhuillier and Quan 2002) are relaxed. Han, Bae, and Ha (2000) introduced a hybrid stereo matching algorithm that integrated the edge-based and area-based methods. During the matching procedure, different matching strategies were adopted, and an adaptive matching window with variable sizes and shapes was used to consider the local textural information. In addition, a new relaxation scheme based on the statistical distribution of matching errors was proposed to efficiently reduce the mismatches in unfavorable conditions. Several constraints, such as disparity smoothness and discontinuity preservation, were employed.

More recently, Zhang (2005) and Zhang and Gruen (2006) developed the Geometrically Constrained Cross-Correlation (GC^3) algorithm to provide a dense pattern of mass points for DSM generation. This algorithm is based on the concept of multi-image matching. A correlation function called the Sum of Normalized Cross-Correlation (SNCC) was introduced to replace NCC for the purpose of reducing the ambiguity caused by occlusions and surface discontinuities. The algorithm has been successfully used in the reality-based generation of virtual environments for digital earth (Gruen 2008). However, this algorithm mainly depends on multiple images. The mismatching probability of SNCC may increase with the decreasing number of images, especially when only two images are available. In order to improve the accuracy of stereo matching, some constraints have been proposed. Silveira et al. (2008) proposed a hybrid matching method which combined a feature-based algorithm with an area-based algorithm. In this method, Scale-invariant feature transform (SIFT) (Lowe 2004) is employed first to provide a set of seed points. Then, LSM with region growing is used in a subsequent step. Finally, a dense and well-distributed cloud of corresponding points on a pair of satellite images is obtained. Although the procedure needs no human intervention, there are some problems: (a) when this method is used in repetitive textural or homogeneous textural areas, the region growing may not obtain dense and robust corresponding points; and (b) since the EOPs of satellite images are known in advance, which can simplify image matching and avoid mismatches, these auxiliary data should be used in the matching method. Zhu, Wu, and Tian (2007) and Wu, Zhang, and Zhu (2011) presented a triangulation-based hierarchical image matching method. This method uses a few seed points to generate initial Delaunay triangulations, and interest points are matched under the triangle and epipolar constraints. Once a pair of corresponding points is obtained, the triangulations are updated and extended dynamically. Even though the triangle constraint is effective in helping to find correct matches in areas with perspective distortions, the epipolar constraint for sensors with frame perspective is not suitable for satellite imagery. Due to the linear array imaging modes of satellites, the corresponding rigorous epipolar lines are not straight lines any more. It is not easy to extract rigorous epipolar lines in satellite imagery directly. Instead, approximate epipolar lines are used for satellite image matching (Ji and Yuan 2010). In addition, Chen and Shao (2013) proposed a novel line-based matching method for high resolution remote sensing images. All the extracted line segments are grouped into salient lines and general lines. The hierarchical strategy employed in the method avoids a mass of iteration. Simioni et al. (2011) proposed a new algorithm for stereo image matching. In this algorithm, snakes are used as a tool to evolve an easy-to-find zero-order estimation of the stereo pair disparity map until an optimum global correspondence between the images is obtained.

3. Algorithmic outline

The proposed method generates the pyramid levels of satellite images. The satellite images are enhanced by a modified Wallis filter, which determines the parameters adaptively and avoids

over-enhancement. The SIFT algorithm is then employed to obtain some initial correspondences on the top level, and a mismatch detection based on a global-local strategy is introduced to remove outliers before a geometric orientation with bundle block adjustment (Zhang, Zheng, and Xiong 2014). After initial orientation, the interest points are detected next, using the Harris detector (Harris and Stephens 1988), after which a hierarchical image matching method is developed to improve the accuracy of matching results, level by level. In this method, the corresponding correlation window is determined by an approximate epipolar constraint and a triangulation constraint, and rectified by an affine transformation model. A novel similarity measure which integrates distance, angle, and NCC similarities (DANCC) is thereafter proposed to find the correct matches. The framework of this method is illustrated in Figure 1.

3.1. Modified Wallis filter

As an image enhancement operator, the Wallis filter (Pratt 1991), which is widely used in photogrammetry, is employed here to enhance and sharpen the texture patterns and increase the

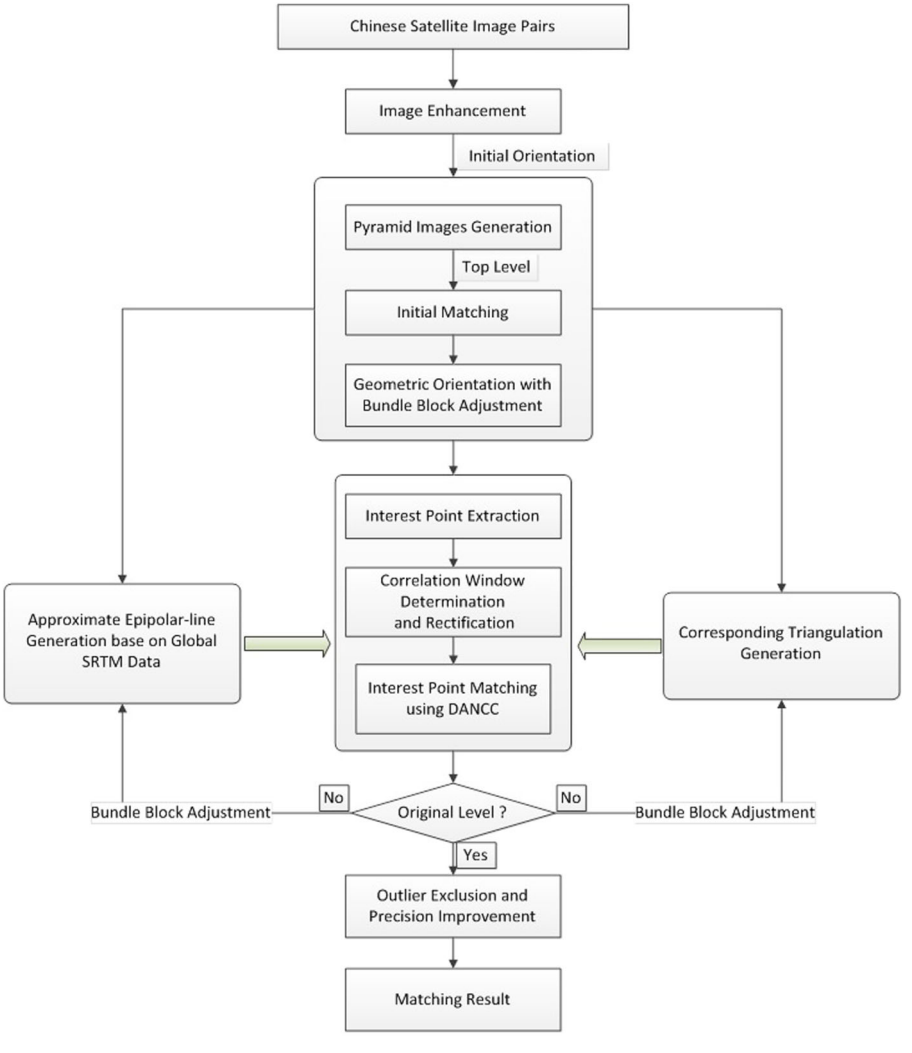

Figure 1. The framework of the proposed matching algorithm.

signal-to-noise ratio (Baltsavias 1991; Wu, Zhang, and Zhu 2011). The general form of the Wallis filter is given in the following equations:

$$\mathbf{g}^{\mathrm{w}}(x, y) = \mathbf{g}(x, y) \cdot r_1 + r_0 \tag{1}$$

$$r_1 = cs_f/(cs_g + s_f/c); \quad r_0 = bm_f + (1 - b - r_1)m_g \tag{2}$$

where $\mathbf{g}^{\mathrm{w}}(x, y)$ is the image after image enhancement; $\mathbf{g}(x, y)$ is the original image; r_0 is the additive parameter; r_1 is the multiplicative parameter; m_g is the mean deviation of original image; s_g is the standard deviation of original image; m_f is the target value for the mean deviation; s_f is the target value for the standard deviation; c is the contrast expansion constant; b is the brightness forcing constant.

However, some problems currently exist for the Wallis filter: (1) there is over-enhancements caused by unreasonable parameters, which may lead to textural information losses and failed noise restraint; and (2) the parameter setting cannot be determined adaptively.

The unreasonable parameters b and c are actually the reason for over-enhancement. Due to the restriction on gray level, unreasonable parameters b and c may lead to excessive losses of gray information. Wallis filter is the method to enhance the dark pixels and preserve the bright pixels at the same time. The choice of parameters b and c is related to the classification of dark pixels and bright pixels, which is actually an image binarization problem. In order to improve the performance of Wallis filter, the optimal parameters b and c can be determined from a self-adaptive image binarization method.

Ostu method was used (Ostu 1979) to get an optimal threshold T. Parameters b and c are calculated in the following equation:

$$\begin{aligned} b &= (255 - T + 1)/255 \\ c &= ((255 - T + 1)/255) + 0.3 \end{aligned} \tag{3}$$

where b is corresponding to the set of dark pixels; c is corresponding to the set of bright pixels. In order to avoid c becoming zero, we added a tiny constant to c, such as 0.3.

To test the performance of the modified Wallis filter, two typical image block patches were used as shown in Figure 2(a). Figure 2(b) shows the results produced by the Wallis filter. It can be seen that the image block patches are over-enhanced, and image noise has increased. From Figure 2(c), the results produced by the modified Wallis filter are satisfactory, and the above problems are overcome effectively.

Wallis filter is a linear transformation, which is used in every level of pyramid images to enhance and sharpen the texture patterns. In order to achieve good matching results, it requires similarity measures to be invariant to linear transformations. Both SIFT and DANCC are used in this paper, which are invariant to linear intensity transformations.

3.2. Initial geometric orientation

Unlike aerial sensors with the central projection, the satellite sensors work in the pushbroom mode and capture linear array images so that the epipolar lines are not straight linesanymore. Because there are large errors of the real-time EOPs, which are due to insufficient knowledge of the satellite attitude as well as thermally influenced mounting angles between the optical sensor and the attitude measurement unit (Rupert et al. 2012), the disparity between the true corresponding points and their corresponding approximate epipolar lines increases. In this case, the approximate epipolar lines may fail to help in finding correct matches.

Initial geometric orientation is a method to improve the accuracy of the EOPs. It needs some good initial correspondences on the top level of pyramid images in advance. After initial geometric orientation, the prediction accuracy of the approximate epipolar lines are improved greatly, and better

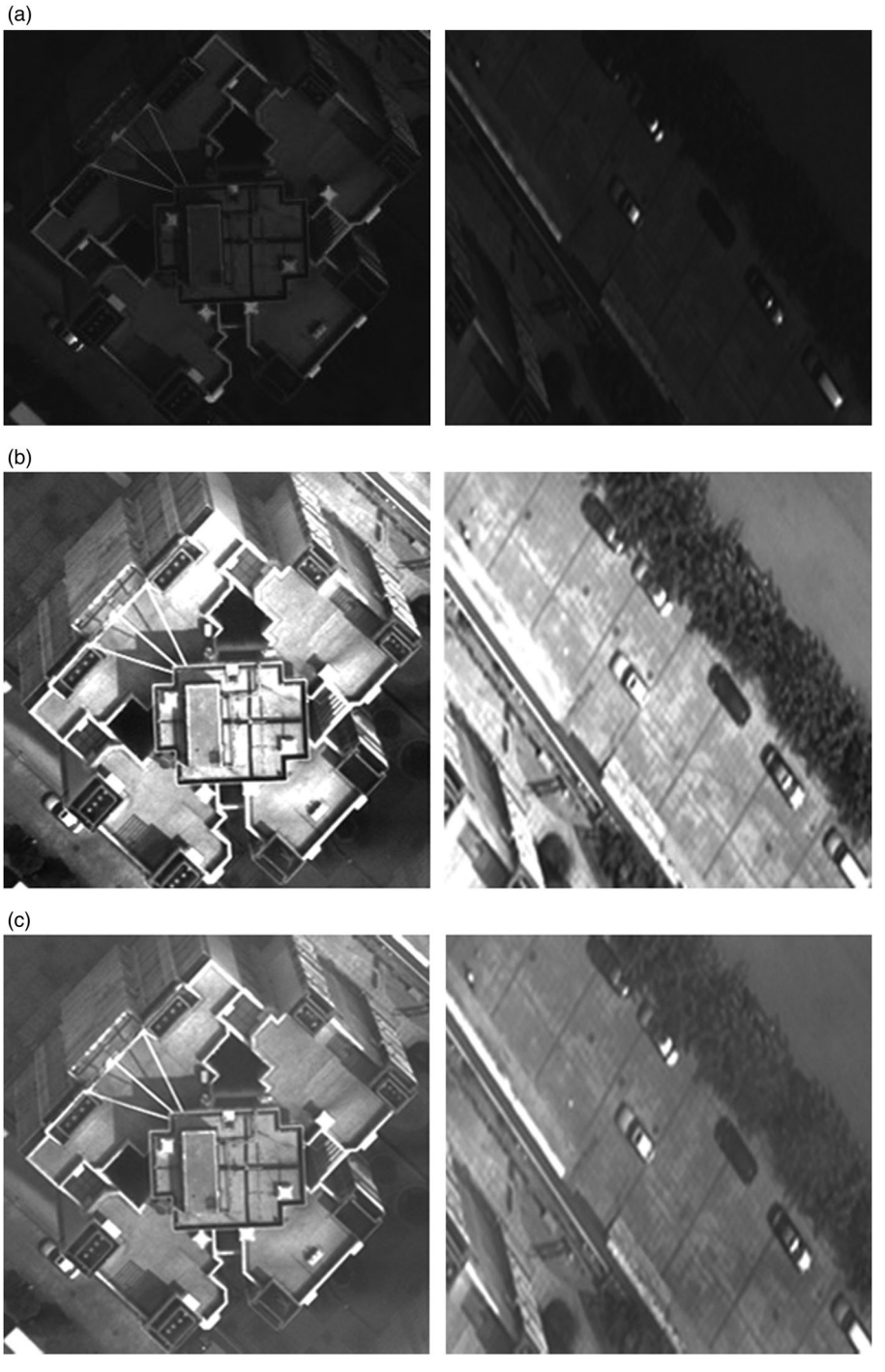

Figure 2. The comparison between the Wallis filter and the modified Wallis filter.

matching results can be expected. There have been several sensor models for initial orientation, such as direct georeferencing model (Yastikli and Jacobsen 2005), the piecewise polynomial model (Hofmann, Nave, and Ebner 1982), the orientation image model (Gruen and Zhang 2002) and the

systematic error compensation model (Kocaman and Gruen 2008). Many additional experiments verified that considerable accuracy could be obtained by adopting the systematic error compensation model and compensating for the constant error of the position and attitude observations (Kocaman and Gruen 2008; Zhang, Zheng, and Xiong 2014; Zheng et al. 2015). As the method of Zhang, Zheng, and Xiong (2014) and Zheng et al. (2015) has been successfully used in bundle with Chinese satellite imagery, this paper employs the systematic error compensation model for the initial orientation.

3.2.1. Mismatch detection based on global-local strategy

SIFT is widely applied today in photogrammetry and remote sensing. It can extract features which are invariant to image scales and rotations and can provide robust but sparse corresponding points (Mikolajczyk and Schmid 2004). In this paper, SIFT is used to find some initial correspondences. Most of the corresponding points are correct matches, but there are still some mismatches that need to be removed to improve the accuracy of geometric orientation.

The mismatch detection method uses a global-local strategy to remove outliers. First, a quadratic polynomial is used as the global fitting model, and all the correspondences are selected to calculate its parameters. Then, the points in the left image are transformed onto the right image through the fitting model, and the deviations are obtained. When the deviation of a correspondence is more than three times of the mean square value, this correspondence is considered to be a mismatch. After the obvious mismatches are removed, bundle block adjustment using a systematic error compensation model is adopted to improve the accuracy of EOPs. The elevation values of each correspondence can also be obtained at the same time. Then, we classify the correspondences through the neighbor space which is established according to the position and elevation relationship between the correspondences. Each neighbor space is considered to be a local region composed of adjacent correspondences with nearly the same elevation values. The local region is assured to be smooth enough. Finally, a random sample consensus strategy is adopted to exclude the outliers (Hartley and Zisserman 2003) within each local region, and an affine transformation model is calculated as the local fitting model. The corresponding points which are unable to satisfy the model are considered to be mismatches. Finally, the bundle adjustment is adopted again to improve the accuracy of geometric orientation further.

3.3. Combined image matching method

A combined image matching method for Chinese satellite imagery is proposed in this paper. This method includes three steps:

(1) After the initial Delaunay triangulations (Zhu et al. 2005) are generated, a series of correlation windows for each interest point are determined along the corresponding approximate epipolar line. The robust approximate epipolar lines are generated by a projection track method based on Shuttle Radar Topography Mission (SRTM) data.
(2) An integrated similarity measure is presented to find correct matches.
(3) A novel hierarchical matching strategy is presented to produce reliable and accurate matching results.

3.3.1. Correlation windows determination

After the initial geometric orientation, some of the robust correspondences are saved. They are used to generate a pair of initial Delaunay triangulations. This paper supposes that each triangle is a locally planar area. However, once the disparities are discontinuous in the same triangle, this assumption may fail. Fortunately, as disparities of the scene are piecewise continuous, the hypothesis is proper in most cases. Once an interest point lies within a triangle with continuous disparities in the left image, its corresponding points should be found along the approximate epipolar line in the

corresponding triangle in the right image, as shown in Figure 3. It is impossible to decide the continuity of each trianglebeforehand; so mismatches cannot be avoided. But triangulation can help to find most correct matches. This paper intends to acquire feature matching points instead of pixel-wise dense matching points. The correspondences of the most feature points are located in the corresponding triangles, and the few mismatches which are caused by the disparity discontinuity within a triangle can be eliminated by outlier detection methods.

In Figure 3, triangles Δabc and $\Delta a'b'c'$ are a pair of corresponding triangles in the left and right images. The piecewise continuous line segments in the right image represent the approximate epipolar line of point $P(x, y)$. The approximate epipolar line is established based on the projection track (Hu et al. 2009). We used SRTM to confirm the elevation range. A projection window centered on point $P(x, y)$ is defined in the left image, and four corners are projected onto the right image according to the post-processed EOPs. Then, a series of correlation windows are established along the approximate epipolar line. Under the triangulation constraint, the correlation windows which overlap with the triangle are available, and their pixels which lie within the triangle are considered to be potential corresponding points. After initial geometric orientation, the accuracy of EOPs has been improved greatly. The distance between a feature point and the corresponding epipolar line can be reduced to at most 10 pixels. In order to get robust matching results, we set a threshold to limit the search range perpendicular to the approximate epipolar line. We set the threshold as 13 pixels in all of the experiments in this paper.

3.3.2. Local geometric distortion rectification

For the satellite image pairs illustrated in Figure 7, there are different spatial resolutions and different perspectives, and the local distortion caused by topographic relief should be considered. These differences may lead to a low correlation when using the NCC method and can form an irregular or discontinuous correlation window as well. Therefore, this paper uses the affine transformation to warp the correlation window.

From Figure 4, an image window Π and a projection window Γin the left image are determined. According to the section on correlation window determination, the affine transformation parameters between the projection window Γ and an arbitrary correlation window Γ_p can be calculated, and the local distortion can be compensated by this transformation. In addition, each correlation window needs to be resampled and the gray values of the pixels in the correlation window are interpolated by a bilinear interpolation method. The affine transformation does not consider discontinuities. However, each projection window is usually small (127×127 pixels in our experiments). In such a small window, depths are considered to be continuous. The assumption works in most terrains where the depths are piecewise continuous.

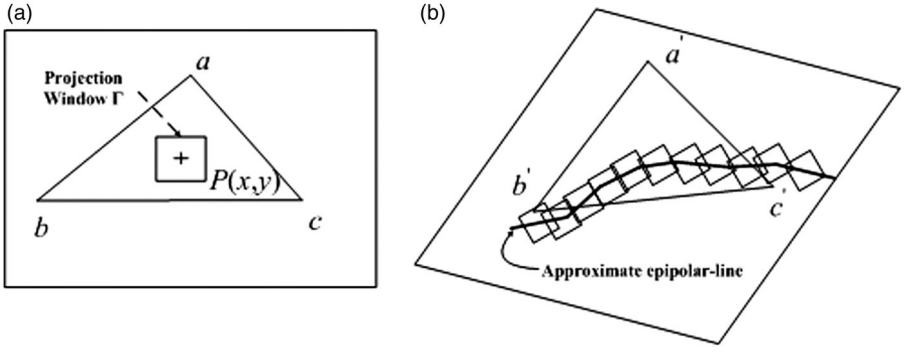

Figure 3. The illustration of correlation windows determination.

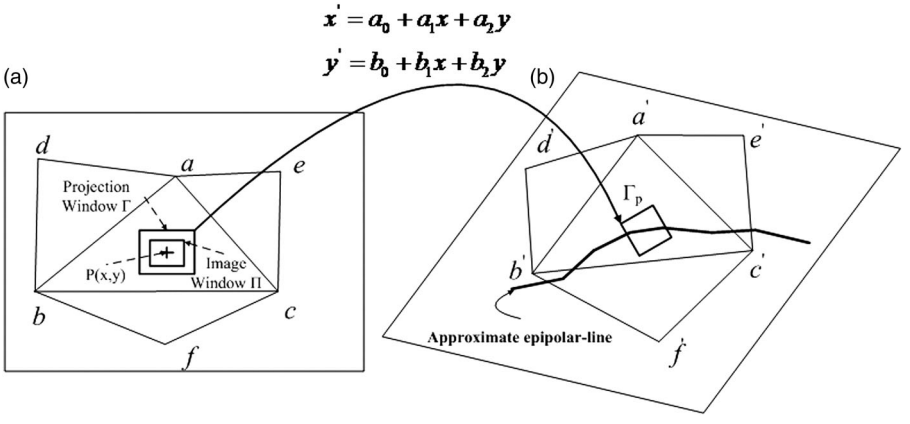

Figure 4. The illustration of local geometric distortion rectification.

3.3.3. An integrated similarity measure (DANCC)

NCC is a main and commonly used measure in satellite image matching. This measure is simple with accurate correspondences; but it only takes the textural similarity into account so geometric similarity is not considered. Therefore, it may be difficult for NCC to find correct matches in repeated textural areas and poor textural areas.

In this paper, a similarity measure that integrates distance vector, angle vector and NCC (DANCC) is presented.

3.3.3.1. Distance vector. Under the triangulation-based constraint, each triangle is considered to be a locally planar area. From Figure 5, the spatial distance between interest point $P(x, y)$ and its closest triangle vertex a in the left image should be equal to the spatial distance between its corresponding point and the triangle vertex a' in the right image. In reality, there is a difference caused by the scale change and the different perspectives. When interest point c lies within triangle Δabc, the difference ΔL can be calculated in Equation (4), where L_{ab} is the length of vertexes a and b. The threshold of the distance vector then is obtained in Equation (5). Each interest point can achieve different thresholds adaptively. The distance vector L_{DV} is represented in Equation (6). In other words, if the distance L' for a potential corresponding point is closer to a threshold than other points, this potential corresponding point has higher

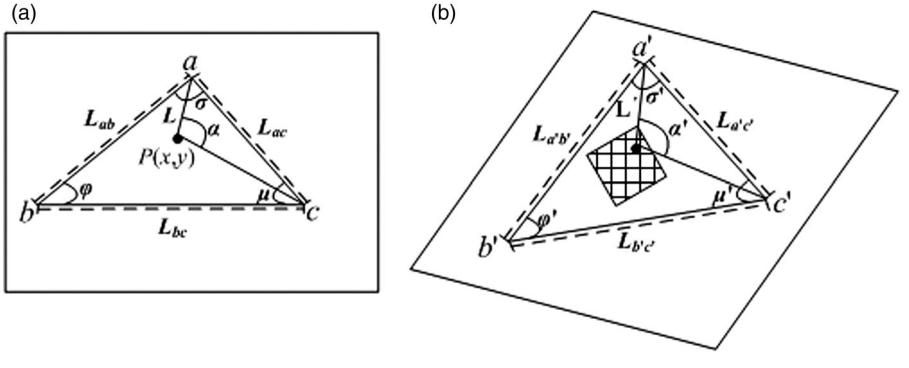

Figure 5. The illustration of distance vector and angle vector.

probability of being a correspondence.

$$\Delta L = \left(\frac{L_{a'b'} - L_{ab}}{L_{ab}} + \frac{L_{a'c'} - L_{ac}}{L_{ac}} + \frac{L_{b'c'} - L_{bc}}{L_{bc}} \right) / 3 \tag{4}$$

$$L_{\text{Threshold}} = L + L \cdot \Delta L \tag{5}$$

$$L_{DV} = (L' - L_{\text{Threshold}})^2 \tag{6}$$

Han et al. (2012) has regarded the spatial distance as a similarity measure. The spatial distance is defined as the distance between feature points and the affine-transformed points, which is later combined with SIFT descriptor. Different from his work, the spatial distance in this paper is between the feature point and the vertex point, and we combine the distance with NCC.

3.3.3.2. Angle vector. Like the distance vector, the angle vector also is used in this similarity measure. From Figure 5, interest point p and its two closest triangle vertexes, *a* and *c*, in the left image form angle α. Under the condition of scale change and rotation between a pair of images, angle α should be consistent with angle α' of its corresponding point in the right image. However, there is actually a difference caused by the surface topographic relief. When interest point $P(x, y)$ lies within triangle Δabc, the difference $\Delta\alpha$ can be calculated in Equation (7), where ϕ is the angle of sides *ab* and *bc*. The threshold of the angle vector is obtained in Equation (8). Each interest point can achieve a different threshold adaptively. The angle vector α_{AV} is represented in Equation (9). In other words, if angle α' for a potential corresponding point is closer to a threshold than other points, this potential corresponding point has a higher probability of being a correspondence.

$$\Delta\alpha = (\varphi' - \varphi + \sigma' - \sigma + \mu' - \mu)/3 \tag{7}$$

$$\alpha_{\text{Threshold}} = \alpha + \Delta\alpha \tag{8}$$

$$\alpha_{AV} = (\alpha' - \alpha_{\text{Threshold}})^2 \tag{9}$$

3.3.3.3. Adaptive Normalized Cross-Correlation (NCC). After correlation window determination and local geometric distortion rectification, the warp for the correlation windows is compensated, and the potential corresponding points are obtained by the approximate epipolar and triangulation constraints. The correlation value for each potential corresponding point can be obtained using NCC. The threshold of NCC is an important parameter which affects the performance of NCC; and in this paper, the threshold is calculated adaptively. The three vertexes of the pair of triangles within which the interest points lie are used to calculate their NCC values. The average NCC value then is obtained. The threshold is set to the subtraction between the average value and a constant. In this paper, the constant was set to 0.1.

3.3.3.4. Similarity measure establishment. The distance vector, angle vector and NCC are assigned to describe each potential corresponding point. The minimum Euclidean distance is employed as the similarity measure, which is described in Equation (10), where *a* and *b* are the weight values of the distance and angle vectors ($0 < a < 1,\ 0 < b < 1,\ 0 < a + b < 1$). Once the NCC value of a potential corresponding point is less than the threshold $\text{NCC}_{\text{Threshold}}$, this point will be removed. The corresponding point for each interest point is determined by

identifying the smallest value $E(x, y)$ among its potential corresponding points.

$$E(x,y)=\begin{cases}\sqrt{a\cdot L_{DV}+b\cdot\alpha_{AV}+(1-a-b)\cdot\left(\dfrac{1}{\mathrm{NCC}-\mathrm{NCC}_{\mathrm{Threshold}}}\right)^{2}} & (\mathrm{NCC}\geq\mathrm{NCC}_{\mathrm{Threshold}})\\ \text{Invalid} & (\mathrm{NCC}<\mathrm{NCC}_{\mathrm{Threshold}})\end{cases} \tag{10}$$

There are two parameters that need to be estimated: the weight a of the distance vector and weight b of the angle vector. As the weight values change, the performance of DANCC will be different. Through a large amount of experiments, we found that the highest correct matching rate was obtained when weight a was set at the range of 0.15–0.2 and weight b was set at the range of 0.35–0.4. In this paper, we set weight a at 0.15 and weight b at 0.35.

DANCC consists of three parts: the distance vector, the angle vector and NCC. According to Equations (6) and (9), the distance vector and the angle vector are only dependent on vertexes of triangles. So both the distance vector and the angle vector are invariant to radiometric distortions, no matter the intensity transformation is linear or nonlinear. NCC is known to be invariant to linear transformations. In general, DANCC inherits the radiometric distortion invariances of the distance vector, the angle vector and NCC. It is able to be as invariant as NCC to linear intensity transformation. Though Wallis filter is a linear transformation, DANCC is not influenced by the intensity transformation.

After both weight values were determined, DANCC was compared with the NCC method to test its performance. Figure 6(a) and 6(b) shows a zoomed view of the image pair shown in Figure 7(a) and 7(b). The correspondence marked with a cross in the left image is an interest point. Figure 6(c) and 6(d) shows the similarity values using NCC and DANCC with different potential corresponding points. From Figure 6(c), it can be seen that when NCC was selected as the similarity measure, there were several potential corresponding points with nearly maximum values, which caused the ambiguity in correspondence determination. In Figure 6(d), when DANCC was selected as the similarity measure, the potential corresponding point with the minimum value was distinct and unique. As displayed in Figure 6(b), the correspondence determined by NCC was an outlier, but the correspondence determined by DANCC was correct and accurate.

3.4. Hierarchical matching strategy

In the matching strategy, interest points are re-extracted and the approximate epipolar lines are updated on each level. The quadratic polynomial fitting model is applied to refine the matching result. After image matching is completed on the top level, bundle block adjustment is used to compensate the errors of the EOPs. The prediction accuracy is improved, and the residuals of all the correspondences are obtained. On the next level, the correspondences on the top level whose residuals are less than three times of the root-mean-square error (RMSE) are saved to generate the triangulation. The post-processed EOPs are used to generate more accurate approximate epipolar lines. Under the epipolar and triangulation constraints, the interest points are re-extracted for matching. The process is repeated level by level until the correspondences on the original level are refined, and the correspondences whose residuals are less than six times of the RMSE are saved as the final matching results.

4. Experiments and analysis

Four typical image pairs, as displayed in Figure 7, were used to evaluate the performance of the proposed method. Figure 7(a) and 7(b) shows a stereo pair which was acquired from the ZY-3 satellite in 2013 in Nanjing, China. The left image was acquired from the forward CCD sensor, and the right image was acquired from the backward CCD sensor. A stereo angle of 44° was yielded between

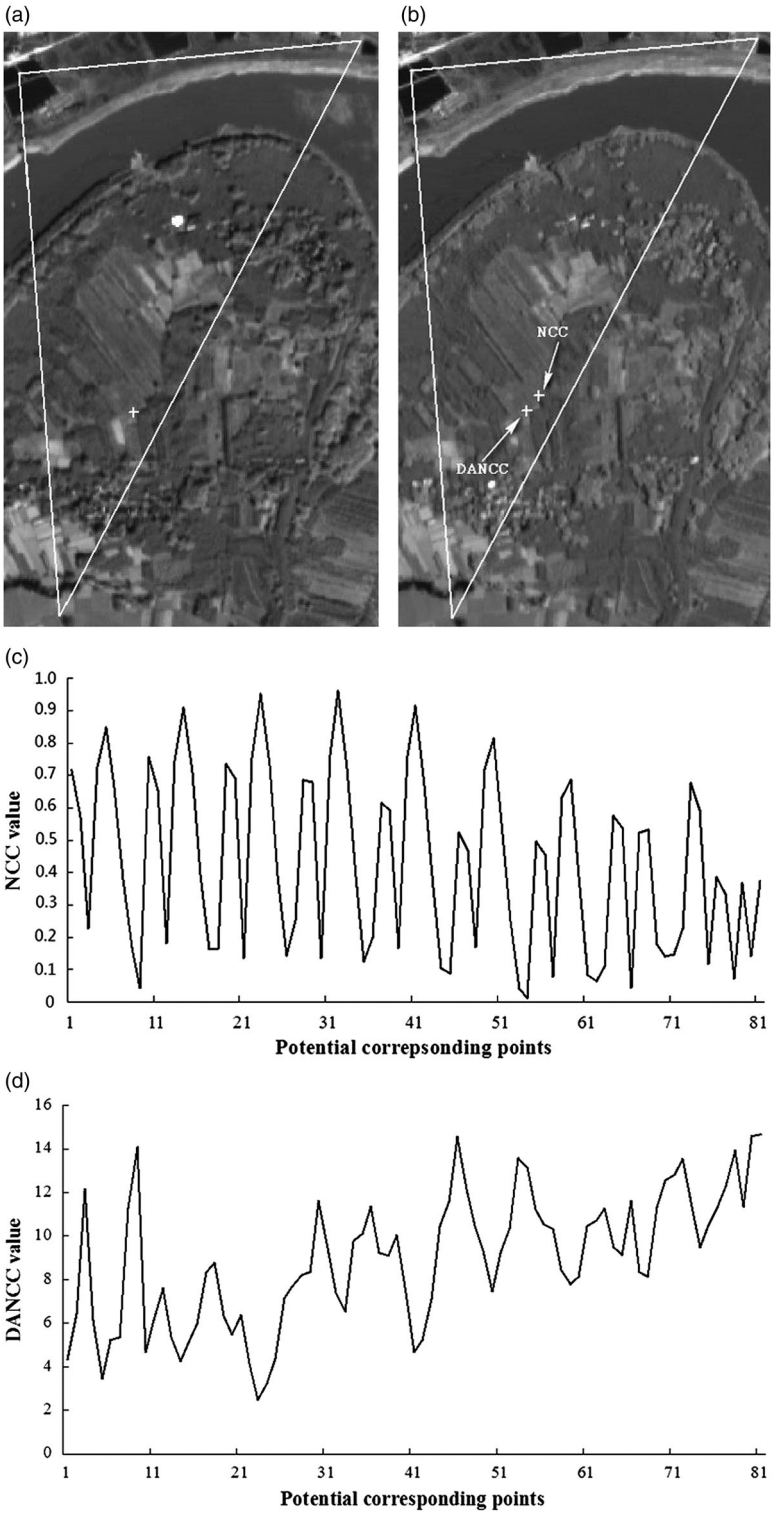

Figure 6. Comparison of different similarity measures: (a) zoomed view of left image, (b) zoomed view of right image, (c) similarity values using NCC and (d) similarity values using DANCC.

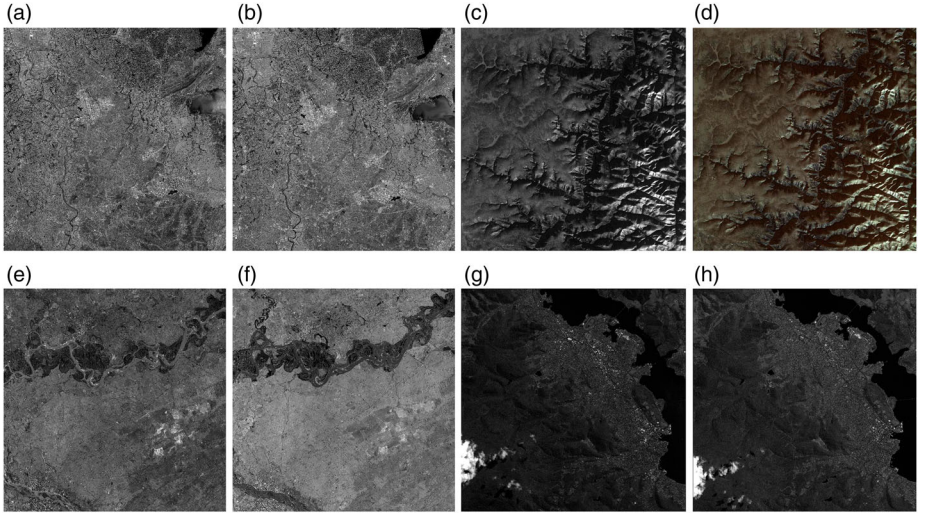

Figure 7. Examples of satellite image pairs.

them. In addition, this pair contained many residential and farmland areas. Figure 7(c) and 7(d) shows an image pair which was acquired from the ZY-1 02C satellite in 2012 in Tommot, The Sakha Republic. The left image was acquired from the panchromatic CCD sensor, and the right image was acquired from the multispectral CCD sensor. The ratio of spatial resolution was about 2. This pair was also a small part of an original long-strip of images containing extensive mountainous areas, in which occlusions and surface discontinuities can be found. Figure 7(e) and 7(f) shows a stereo pair acquired from Mapping Satellite-1. The left image was acquired from the forward CCD sensor, and the right image was acquired from the backward CCD sensor. A stereo angle of 50° was yielded between them, and different terrains were present. To estimate the applicability of our work to foreign satellite imagery, an image pair with different imaging time acquired from GeoEye-1 was selected as shown in Figure 7(g) and 7(h).

The two main methods for matching satellite images were used in this evaluation: the GC^3 method (Zhang 2005; Zhang and Gruen 2006), in which NCC is used as the similarity measure under the epipolar constraint; and the triangulation-based hierarchical matching method (TAACC) (Wu, Zhang, and Zhu 2011), in which the triangulation constraint is developed to help find correct matches. Both of the methods have been used for matching of Chinese satellite imagery (Tong et al. 2015; Wu et al. 2011; Zhang et al. 2014).

To quantitatively analyze the performance of the matching methods, accurate EOPs of the test images were obtained by a long-strip bundle block adjustment with GCPs (Zhang, Zheng, and Xiong 2014) in Tests 1. The spatial forward intersection was adopted to achieve the object 3D coordinates of all the correspondences. Then, the 3D coordinates were backward projected onto the image space, and their statistics of RMSE in image space were obtained as the matching performance indicator. In Test 2, the successful rate of matching was estimated, and 2000 correspondences were selected randomly for use as checkpoints to manually measure the mismatching rate. In Test 3, the matching results produced on different terrains were analyzed, and the proposed method was evaluated. Test 4 aimed at estimating the applicability of the proposed method to foreign satellite imagery.

4.1. Experimental results of Test 1

The stereo pair illustrated in Figure 7(a) and 7(b) was adopted as the test data in Test 1. There were still systematic errors in the original EOPs. The proposed method, GC^3, and TAACC were used to

produce the correspondences between both images. Test 1 aimed at testing the performance of the three methods when the systematic errors of the original EOPs existed. GC^3 only used approximate epipolar lines to predict potential correspondences. TAACC combined triangulation and epipolar

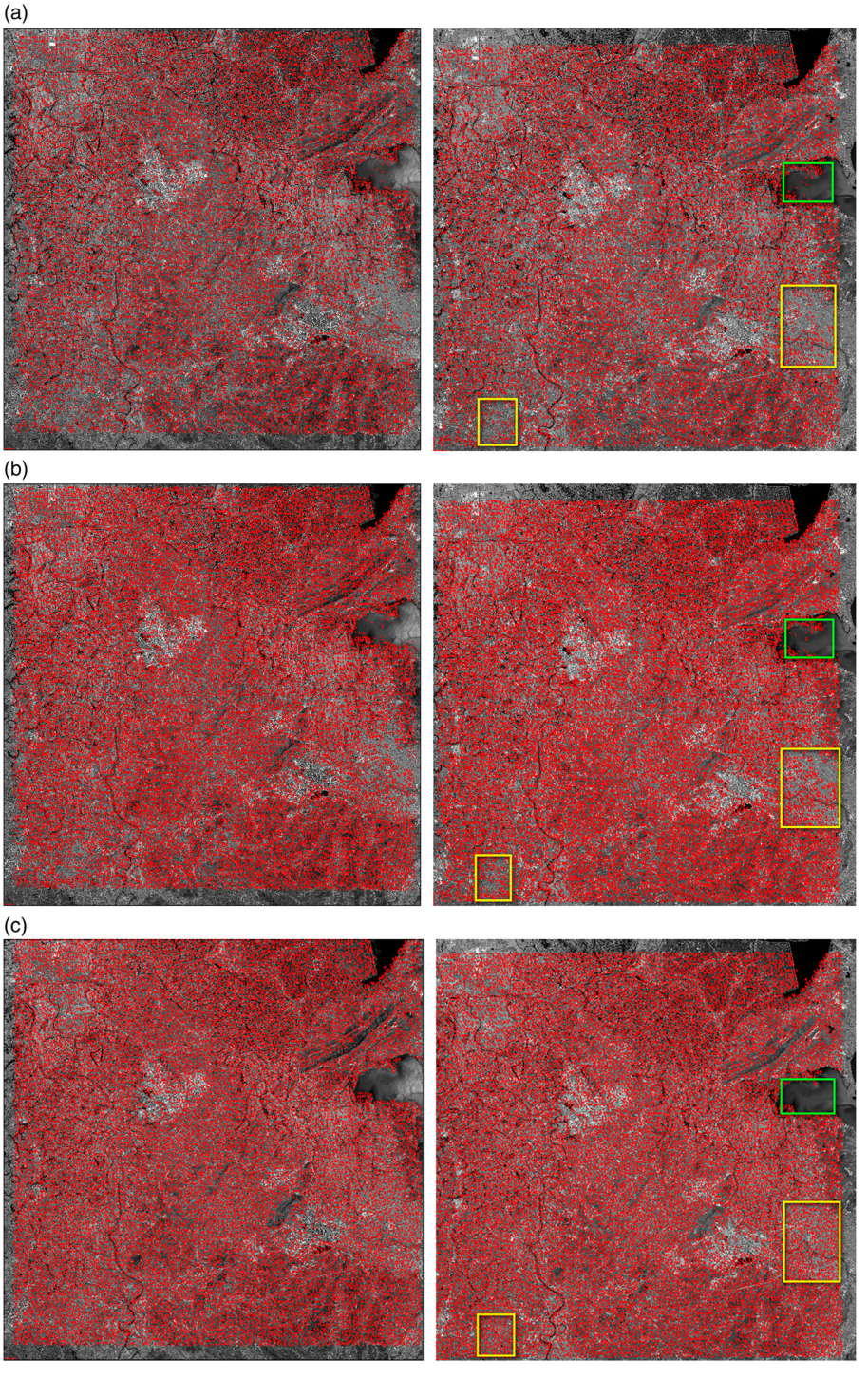

Figure 8. Comparison of the matching results produced by the three methods for ZY-3 satellite imagery.

Table 1. Experimental results produced by GC3, TAACC and the proposed method.

Matching method	Interest points	Matching points	Max difference in image horizontal direction (Pixel)	Max difference in image vertical direction (Pixel)	RMSE (Pixel)
GC^3	46,600	22,483	12.45	9.43	1.22
TAACC	46,600	32,576	4.13	2.82	0.64
Proposed method	46,600	35,892	3.23	2.77	0.43

constraints together to find correspondences. The proposed method used refined epipolar lines and triangulation constraints to predict potential correspondences. To ensure that the comparison was conducted under the same conditions, the parameters for the three methods were identical. For instance, the number of interest points was 46,600 and the layer number of pyramid levels was three.

Figure 8(a) shows the matching result produced by GC^3. This method was constrained by the approximate epipolar lines, but the systematic errors of the original EOPs existed, which caused the prediction of approximate epipolar lines to be inaccurate. Even though the hierarchical matching strategy was used to reduce the influence of prediction error, the successful rate of matching was not improved. Table 1 shows the accuracy evaluation of the three methods. The first column lists the names of the three methods. The second column shows the number of interest points. The third column shows the number of matching points. The fourth row and the fifth row show the max differences in horizontal and vertical directions, respectively. The difference was the distance between the original matching point and the corresponding projected point. RMSE in the sixth column was the RMSE of all the differences. Table 1 indicates that only 22,483 correspondences were found, and the RMSE was 1.22 pixels, which showed that the low prediction accuracy of approximate epipolar lines will decrease the matching accuracy. So more constraints are needed to improve the matching accuracy further. In Figure 8(b), the matching results produced by TAACC are shown; and as can be seen, denser matching distribution was obtained. This method used the triangulation and epipolar constraints, and although the epipolar constraint was not robust enough to help correct the matches for the satellite images, the triangle-based disparity and gradient orientation derived from the triangulation constraint were effective in finding correspondences. Table 1 shows that 32,576 correspondences were found, and the RMSE was 0.64 pixel, which was better than the GC^3 method. The matching results produced by the proposed method are shown in Figure 8(c). The proposed method used geometric orientation with bundle block adjustment and global SRTM data to refine the prediction accuracy of the approximate epipolar lines, level by level, which strengthened the epipolar constraint. The triangulation constraint was employed, and DANCC replaced the NCC method. Table 1 indicates 35,892 correspondences were found, and the RMSE reached 0.43 pixel. In addition, the area marked using a green rectangle was covered with water, which was the area where the mismatches were concentrated. The areas marked using a yellow rectangle were covered with homogeneous texture patterns, in which corresponding points were difficult to find. Compared with GC^3 and TAACC, the proposed method avoided mismatches in the water area and obtained denser matches in the homogeneous textural areas. Both max differences in horizontal and vertical directions of the proposed method were lowest, compared with the other two methods. It is because the proposed method adopted the improved epipolar constraint and the triangulation constraint, which was helpful to reduce the search range of potential correspondences. These results indicate that the proposed method with higher prediction accuracy of epipolar and triangulation constraints performed better than the other two methods for Chinese satellite imagery.

4.2. Experimental results of Test 2

The image pair shown in Figure 7(c) and 7(d) was used as test data in Test 2. There were different spectral characters between the image pair, and the ratio of spatial resolution was about 2. Furthermore, the images contained extensive mountainous areas, which presented a challenge to the

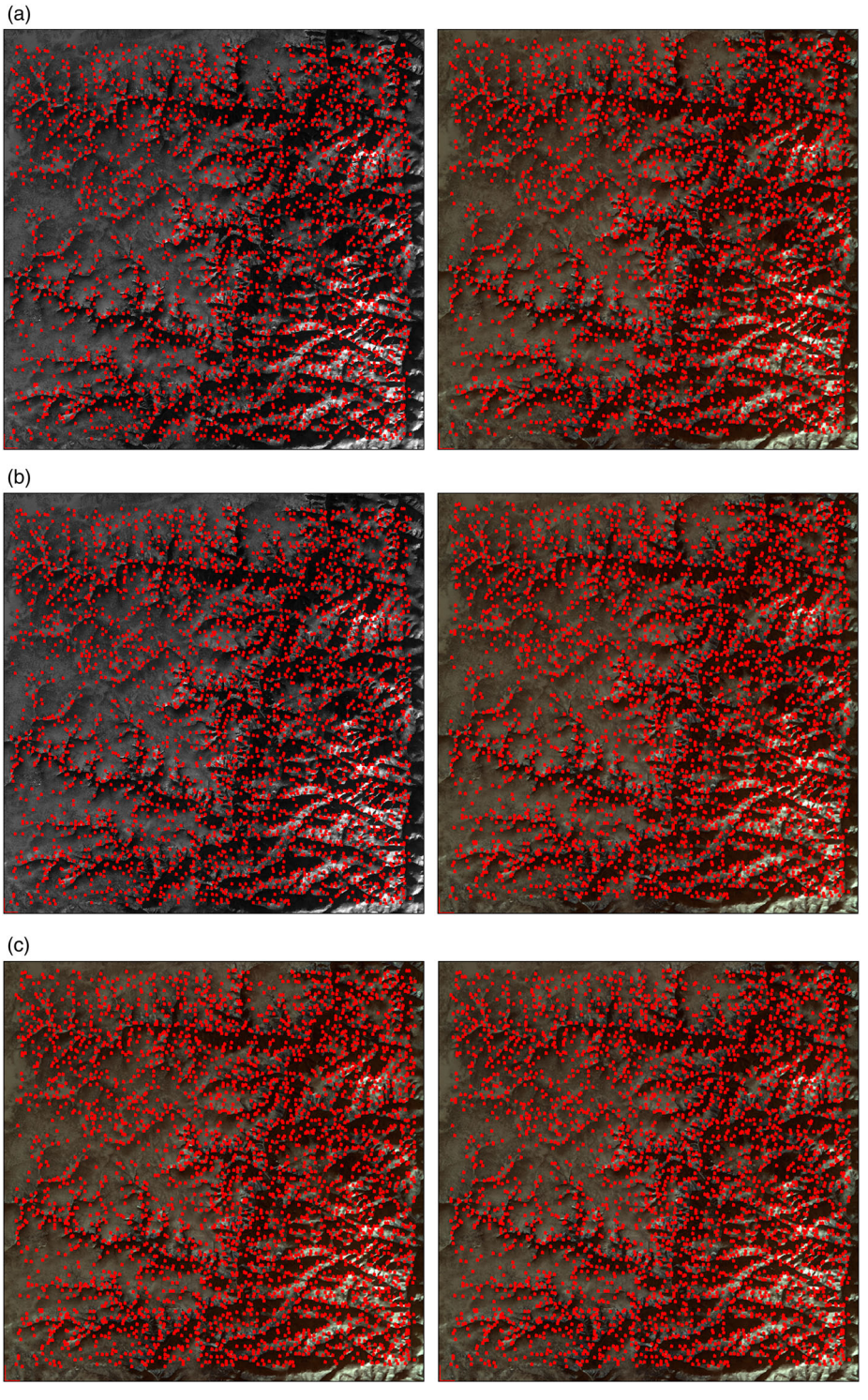

Figure 9. Comparison of the matching results produced by the three methods for ZY-1 02C satellite imagery.

matching stability. The success rate of matching was used as the indicator of matching performance. To measure the validity of the matching methods, 2000 correspondences were selected randomly, which were taken as checkpoints for manual measurement. We divided the image into blocks for even distribution of checkpoints, and then selected checkpoints by a random function in each block. Once the difference of a correspondence between the manual measuring position and the matching position in the image space was more than 1.5 pixels, this correspondence was considered to be a mismatch.

Figure 9(a) and 9(b) shows the matching results produced by GC^3 and TAACC. It can be seen that their matching distributions were both concentrated on the ridge lines. Very sparse correspondences were obtained in poor textural areas and areas with mountain shadows. There are two explanations for this problem. (1) Since GC^3 and TAACC use NCC as their similarity measure, the textural correlation is important in the search for matching points. However, the different spectral properties reduce the textural correlation between the image pair, which may affect the successful rate of matching. (2) In poor textural areas and areas with mountain shadows, the texture patterns still exist, but the textural correlation is low. Although the approximate epipolar lines and the triangulations provide reliable constraints, it is difficult to find matches with high correlation with the NCC method, and may be ineffective in these areas.

Figure 9(c) shows the matching result produced by the proposed method. Denser matching distribution was obtained; and because the distance vector and angle vector were combined with NCC, the textural correlation and the geometric similarity were considered in the search for matches. In addition, the threshold was calculated adaptively in neighbor spaces, which provided a rational restriction in areas with high correlation and low correlation. Table 2 shows that the proposed method attained a higher number of correspondences than the other two methods. Some correspondences were found in poor textural areas and areas with mountain shadows; and the mismatching rate, which was calculated through manual measurement, was lower than the other two methods.

4.3. Experimental results of Test 3

The stereo pair shown in Figure 7(e) and 7(f) was used as test data in Test 3. To estimate the stability of the proposed method to different terrains, areas such as farmland, woodland, and residential regions were selected as well as poor textural areas, all of which were difficult to be matched, as shown in Figure 10. In this test, the interest points were classified by the terrains on which they lay. The success rates and mismatching rates for different terrains are listed in Table 3. It is worth noting that when the error of a correspondence was more than three times of the RMSE, this correspondence was considered to be a mismatch. From Table 3, the results analysis is as follows:

(1) For farmland areas, which have strong texture repeatability, the average success rate was more than 85%, and the average mismatching rate was lower than 4.5%. It can be seen that the proposed method demonstrated good performance in the areas with repeated texture patterns.
(2) For woodland areas, because the texture patterns were too homogeneous, the success rate dropped to below 70%. Moreover, there were several obvious mismatches which increased the mismatching rate, but the average mismatching rate was lower than 11%, which meant that most of the correspondences were correct.

Table 2. Experimental results produced by GC3, TAACC and the proposed method.

Matching method	Interest points	Matching points	Successful rate (%)	Check points	Mismatching rate (%)
GC^3	6147	3360	54.6	2000	9.2
TAACC	6147	3652	59.4	2000	6.9
Proposed method	6147	4529	73.6	2000	3.7

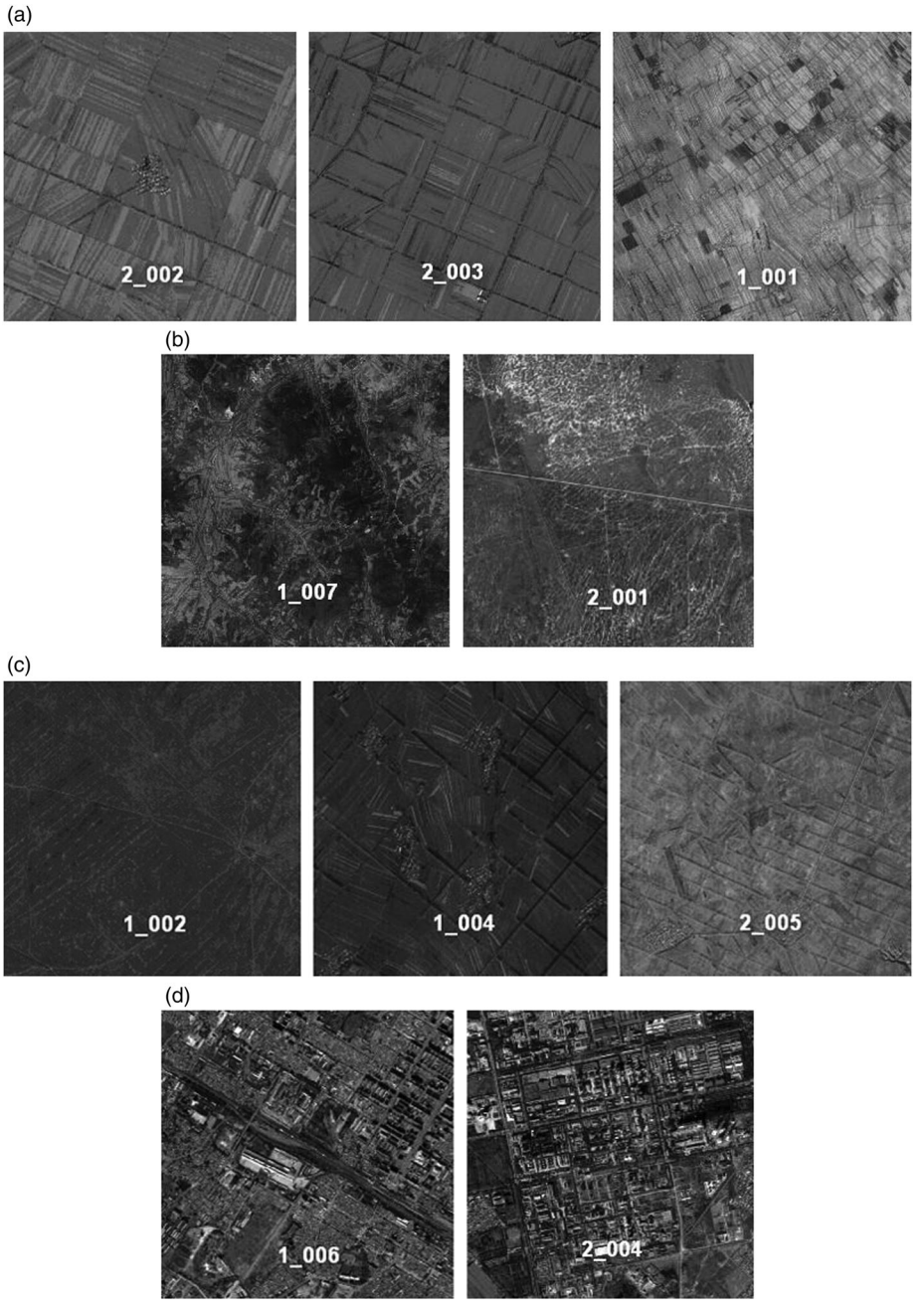

Figure 10. Examples of different terrains for Mapping Satellite-1 imagery.

(3) For residential areas, due to different imaging perspectives, the local distortion was large, but the matching performance remained satisfactory.
(4) For the poor textural areas, the matching results indicated that the proposed method could avoid the matching ambiguity caused by poor textures.

Table 3. Matching accuracy quantitative evaluation for different terrains.

Terrain type	Image block patch	Interest points	Matching points/mismatches	Successful rate/mismatching rate (%)
Farmland area	1_001	106	94/4	88.6/4.2
	2_002	119	108/6	90.7/5.5
	2_003	84	70/2	83.3/2.8
Woodland area	1_007	32	22/2	68.7/9.0
	2_001	26	16/2	61.5/12.5
Residential area	1_006	103	80/5	77.6/6.2
	2_004	94	66/5	70.2/7.5
Poor textural area	1_002	76	52/3	68.4/5.7
	1_004	73	51/3	69.8/5.8
	2_005	66	48/2	72.7/4.1

4.4. Experimental results of Test 4

To estimate the applicability of the proposed method to foreign satellite imagery, the image pair shown in Figure 7(g) and 7(h) was used as test data in Test 4. There was different imaging time between this pair. The success rate of matching is used as the indicator of matching performance. To measure the validity of the matching methods, 2000 correspondences were selected randomly, which were taken as checkpoints for manual measurement. Once the difference of a correspondence between the manual measuring position and the matching position in the image space was more than 1.0 pixel, this correspondence was considered to be a mismatch.

Figure 11 shows the matching result produced by the proposed method. In general, for the foreign satellite imagery, the textural information was more abundant than Chinese satellite imagery. Moreover, the direct georeferencing accuracy using the original position and attitude data was also higher. These advantages help image matching easier. Therefore, the proposed method should produce better matching result for foreign satellite imagery when compared with Chinese satellite. Table 4 confirms the above analysis. The mismatching rate can reach 3.0%. However, the mismatching rate is 3.7% for Chinese satellite imagery, as shown in Table 2.

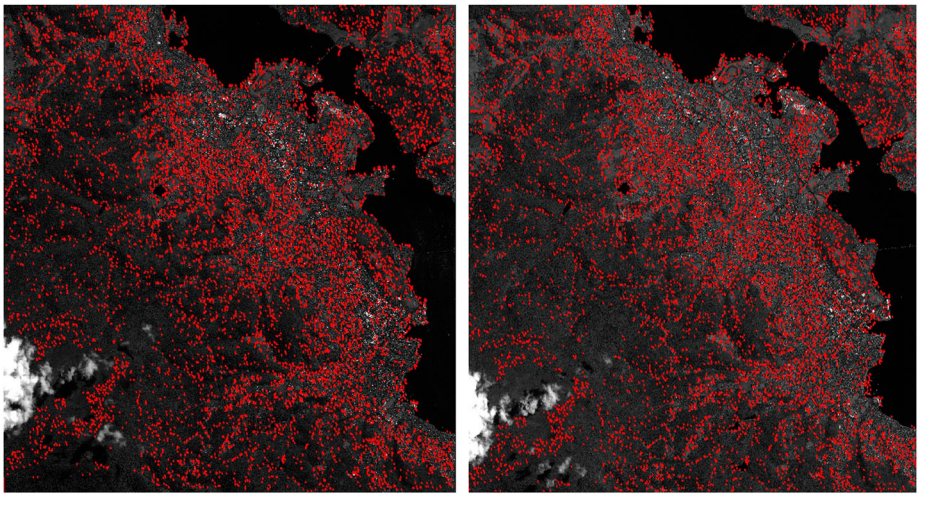

Figure 11. The matching result produced by the proposed method for GeoEye-1 satellite imagery.

Table 4. Experimental result produced by the proposed method.

Matching method	Interest points	Matching points	Successful rate (%)	Check points	Mismatching rate (%)
Proposed method	17,391	13,130	75.5	2000	3.0

5. Conclusions

This paper presented a combined image matching method for Chinese satellite imagery. Three typical image pairs acquired from different Chinese satellites and one stereo pair from GeoEye-1 were used for experimental analysis. Our conclusions are as follows:

(1) The Wallis-type filter developed in this paper can avoid over-enhancement, from which the parameters can be determined adaptively, thereby improving the effect of image enhancement and increasing the success rate of matching.
(2) After the initial correspondences were obtained by the SIFT algorithm, mismatch detection based on a global-local strategy was introduced to remove outliers effectively. Geometric orientation with bundle block adjustment was employed to improve the accuracy of the EOPs, which was ideal for shrinking the searched space and strengthening the approximate epipolar constraint in the matching procedure.
(3) Under the approximate epipolar constraint and triangulation constraint, an integrated similarity measure (DANCC) was presented. This measure considers geometric similarity and textural similarity and demonstrated good performance even in areas with repeated texture patterns and poor textures.
(4) A novel hierarchical matching strategy was introduced, by which the bundle block adjustment was employed, interest points were re-extracted, and the approximate epipolar lines and triangulations were updated, level by level, until a quadratic polynomial fitting model was applied to refine the matching points on the original level. Reliable and accurate matching results were obtained. The hierarchical matching strategy can achieve good matching results even though there are large errors in EOPs. A combination of the improved epipolar constraint and the triangulation constraint is used to reduce the searching range of potential correspondences, which is helpful to improve the accuracy of matching.

Experimental results showed that the method proposed in this paper was able to acquire densely and evenly matching results for different Chinese satellite imagery, including ZY-3, ZY-1 02C, Mapping Satellite-1 and so on. The matching results was robust, even under the condition of residential, farmland and mountain areas. Compared with the two current popular methods, the performance of the new method was better for Chinese satellite imagery. Test 4 showed that the proposed method could also acquire good matching results for foreign satellite images.

Future research will focus on denser matching and improvement of the matching efficiency. The proposed method will be developed for use with a greater array of remote sensors, which will be helpful for further DSM generation and 3D modeling applications using multi-source data. Besides, in order to show the generality of the method, we plan to test the new method with more foreign satellite data.

Acknowledgements

This work was supported in part by the National Natural Science Foundation of China under Grant 41322010 and 41571434, the National Hi-Tech Research and Development Program under Grant 2013AA12A401, and the academic award for excellent Ph.D. Candidates funded by Ministry of Education of China under Grant 5052012213002. Heartfelt thanks are also given for the comments and contributions of anonymous reviewers and members of the editorial team.

Disclosure statement

No potential conflict of interest was reported by the authors.

References

Ackermann, F. 1984. "High Precision Digital Image Correlation." Proceedings of the 39th Photogrammetric Week, Stuttgart, Germany, September 19–24, 231–243.

Baltsavias, E. P. 1991. "Multiphoto Geometrically Constrained Matching." Ph.D. diss., Mitteilungen Nr. 49, Institute of Geodesy and Photogrammetry, ETH Zurich.
Chen, M., and Z. Shao. 2013. "Robust Affine-invariant Line Matching for High Resolution Remote Sensing Images." *Photogrammetric Engineering & Remote Sensing* 79 (8): 753–760.
Cheng, C. Q., K. Z. Deng, Y. S. Sun, and X. T. Li. 2010. "Study of Block Adjustment for Long-strip Satellite CCD Images." *Acta Geodaetica et Cartographica Sinica* 39 (2): 162–168.
Goodchild, M. F. 2008. "The Use Cases of Digital Earth." *International Journal of Digital Earth* 1 (1): 31–42.
Gruen, A. 2008. "Reality-based Generation of Virtual Environments for Digital Earth." *International Journal of Digital Earth* 1 (1): 88–106.
Gruen, A. 2012. "Development and Status of Image Matching in Photogrammetry." *The Photogrammetric Record* 27 (137): 36–57.
Gruen, A., and E. P. Baltsavias. 1988. "Geometrically Constrained Multiphoto Matching." *Photogrammetric Engineering & Remote Sensing* 54 (5): 633–641.
Gruen, A., and L. Zhang. 2002. "Sensor Modeling for Aerial Mobile Mapping with Three-Line-Scanner (TLS) Imagery." *International Archives of the Photogrammetry, Remote Sensing and Spatial Information Science* 32: 85–98.
Guo, H. 2012. "China's Earth Observing Satellites for Building a Digital Earth." *International Journal of Digital Earth* 5 (3): 185–188.
Han, K. P., T. M. Bae, and Y. H. Ha. 2000. "Hybrid Stereo Matching with a New Relaxation Scheme of Preserving Disparity Discontinuity." *Pattern Recognition* 33 (5): 767–785.
Han, Y. K., Y. G. Byun, J. W. Choi, D. Y. Han, and Y. Kim. 2012. "Automatic Registration of High-resolution Images Using Local Properties of Features." *Photogrammetric Engineering and Remote Sensing* 78 (3): 211–221.
Harris, C., and M. Stephens. 1988. "A Combined Corner and Edge Detector." Proceedings of Fourth Alvey Vision Conference, Manchester, 147–151.
Hartley, R., and A. Zisserman. 2003. *Multiple View Geometry in Computer Vision*, 2nd ed. Cambridge: Cambridge University Press.
Helava, U. V. 1978. "Digital Correlation in Photogrammetric Instruments." *Photogrammetria* 34: 19–41.
Heipke, C. 1996. "Overview of Image Matching Techniques." In OEEPE Workshop on the Application of Digital Photogrammetric Workstations, Lausanne, Switzerland, March, URL: http://phot.epfl.ch/workshop/wks96/art_3_1.html.
Hofmann, O., P. Nave, and H. Ebner. 1982. "DPS—A Digital Photogrammetric System for Producing Digital Elevation Models and Orthophotos by Means of Linear Array Scanner Imagery." *International Archives of Photogrammetry and Remote Sensensing* 24: 216–227.
Hu, F., M. Wang, D. Li, S. Jin, and M. Li. 2009. "Generation of Approximate Epipolar Images from Linear Pushbroom Satellite Stereo-imagery Based on Projection Reference Plane." *Acta Geodaetica et Cartographica Sinica* 38 (5): 428–436.
Ji, S. P., and X. X. Yuan. 2010. "Automatic Matching of High Resolution Satellite Images Based on RFM." *Acta Geodaetica et Cartographica Sinica* 39 (6): 592–598.
Joz, W., C. Chi, T. Hsien-Yu, and L. Ming-Che. 2012. "Registration of Multisource Satellite Images by Thin-plate Splines with Highly Reliable Conjugate Points." *Photogrammetric Engineering & Remote Sensing* 78 (6): 583–593.
Kocaman, S., and A. Gruen. 2008. "Orientation and Self-calibration of ALOS PRISM Imagery." *The Photogrammetric Record* 23 (123): 323–340.
Lhuillier, M., and L. Quan. 2002. "Match Propagation for Image-based Modeling and Rendering." *IEEE Transactions on Pattern Analysis and Machine Intelligence* 24 (8): 1140–1146.
Lowe, D. G. 2004. "Distinctive Image Features from Scale-Invariant Keypoints." *International Journal of Computer Vision* 60 (2): 91–110.
Mikolajczyk, K., and C. Schmid. 2004. "Scale & Affine Invariant Interest Point Detectors." *International Journal of Computer Vision* 60 (1): 63–86.
Mustaffar, M., and H. L. Mitchell. 2001. "Improving Area-based Matching by Using Surface Gradients in the Pixel Co-ordinate Transformation." *ISPRS Journal of Photogrammetry and Remote Sensing* 56 (1): 42–52.
Ostu, N. 1979. "A Threshold Selection Method from Gray-Level Histograms." *IEEE Transactions on System, Man and Cybernetics* 9 (1): 62–66.
Pratt, W. K. 1991. *Digital Image Processing*. New York, NY: John Wiley & Sons.
Rupert, M., K. Thomas, S. Mathias, and R. Peter. 2012. "Automated Georeferencing of Optical Satellite Data with Integrated Sensor Model Improvement." *Photogrammetric Engineering & Remote Sensing* 78 (1): 61–74.
Silveira, M. T., R. Q. Feitosa, K. Jacobsen, J. L. N. S. Brito, and Y. Heckel. 2008. "A Hybrid Method for Stereo Image Matching." *The International Archives of the Photogrammetry, Remote Sensing and Spatial Information Sciences, Beijing, China* XXXVII: 895–901.
Simioni, E., N. Giampiero, F. Gianfranco, C. Gabriele, D. D. Vania, M. Matteo, and S. Elisa. 2011. "A New Stereo Algorithm Based on Snakes." *Photogrammetric Engineering & Remote Sensing* 77 (5): 1–13.
Srinivasa, G. N., and K. N. Shree. 2002. "Vision and the Atmosphere." *International Journal of Computer Vision* 48 (3): 233–254.

Tong, X., L. Li, S. LiuY. Xu, Z. Ye, Y. Jin, F. Wang, and H. Xie. 2015. "Detection and Estimation of ZY-3 Three-line Array Image Distortions Caused by Attitude Oscillation." *ISPRS Journal of Photogrammetry and Remote Sensing* 101: 291–309.

Wu, B., J. Guo, Y. Zhang, and B. A. King. 2011. "Integration of Chang'E-1 Imagery and Laser Altimeter Data for Precision Lunar Topographic Modeling." *Geoscience and Remote Sensing* 49 (12): 4889–4903.

Wu, B., Y. S. Zhang, and Q. Zhu. 2012. "Integrated Point and Edge Matching on Poor Textural Images Constrained by Self-adaptive Triangulations." *ISPRS Journal of Photogrammetry and Remote Sensing* 68: 40–55.

Wu, B., Y. S. Zhang, and Q. Zhu. 2011. "A Triangulation-based Hierarchical Image Matching Method for Wide-baseline Images." *Photogrammetric Engineering & Remote Sensing* 77 (7): 695–708.

Xie, J. F. 2009. "The Critical Technology of Data Processing of Satellite Attitude Determination Based on Star Sensor." PhD diss., State Key Laboratory for Information Engineering in Surveying Mapping and Remote Sensing, Wuhan University.

Yastikli, N., and K. Jacobsen. 2005. "Direct Sensor Orientation for Large Scale Mapping-Potential, Problems, Solutions." *Photogrammetric Record* 20: 274–284.

Zhang, L. 2005. "Automatic Digital Surface Model (DSM) Generation from Linear Array Images." PhD. diss., Institute of Geodesy and Photogrammetry, Swiss Federal Institute of Technology Zurich.

Zhang, Y. J., Bo Wang, Z. Zhang, Y. Duan, Y. Zhang, M. Sun, and S. Ji. 2014. "Fully Automatic Generation of Geoinformation Products with Chinese ZY-3 Satellite Imagery." *The Photogrammetric Record* 29 (148): 383–401.

Zhang, L., and A. Gruen. 2006. "Multi-image Matching for DSM Generation from IKONOS Imagery." *ISPRS Journal of Photogrammetry and Remote Sensing* 60 (3): 195–211.

Zhang, Y. J., M. T. Zheng, and J. X. Xiong. 2014. "On-orbit Geometric Calibration of ZY-3 Three-line Array Imagery with Multistrip Data Sets." *IEEE Transactions on Geoscience and Remote Sensing* 52 (1): 224–234.

Zhang, Y. J., M. T. Zheng, X. D. Xiong, and J. X. Xiong. 2015. "Multistrip Bundle Block Adjustment of ZY-3 Satellite Imagery by Rigorous Sensor Model Without Ground Control Point." *IEEE Geoscience and Remote Sensing* 12 (4): 865–869.

Zheng, M. T., Y. J. Zhang, J. F. Zhu, and X. D. Xiong. 2015. "Self-Calibration Adjustment of CBERS-02B Long-strip Imagery." *IEEE Transactions on Geoscience and Remote Sensing* 53 (7): 3847–3854.

Zhu, Q., B. Wu, and Y. X. Tian. 2007. "Propagation Strategies for Stereo Image Matching Based on the Dynamic Triangle Constraint." *ISPRS Journal of Photogrammetry & Remote Sensing* 62: 295–308.

Zhu, Q., J. Zhao, H. Lin, and J. Y. Gong. 2005. "Triangulation of Well-defined Points as a Constraint for Reliable Image Matching." *Photogrammetric Engineering & Remote Sensing* 71 (9): 1063–1069.